Effect of the TBP and Water on the Complexation of Uranyl Nitrate and the Dissolution of Nitric Acid into Supercritical CO_2. A Theoretical Study

R. Schurhammer and G. Wipff*

Institut de Chimie - 4, rue Blaise Pascal 67070 Strasbourg France

Received: March 1, 2005; In Final Form: April 18, 2005

We report theoretical studies on the complexation of uranyl nitrate and the dissolution of nitric acid in supercritical CO_2 by TBP. According to quantum mechanical calculations, TBP (modeled by trimethyl phosphate TMP) displays stronger hydrogen-bonding interactions with HNO_3 than with H_2O, and this has been modeled in force-field calculations. Different combinations of water, TBP, and acid are compared in SC−CO_2 and simulated by molecular dynamics (MD), demonstrating the importance of TBP and water concentrations. In MD simulations, which started from "random" mixtures of water, TBP, nitric acid, and uranyl nitrate, complexation of uranyl by TBP is observed and the yield increases with the TBP concentration. TBP molecules are also necessary to dissolve nitric acid in the supercritical phase. Indeed, without TBP, nitric acid alone self aggregates via hydrogen-bonding interactions. Adding water to this solution leads to the formation of water microdomains containing the acid and uranyl salts. The simulations show that a high TBP/nitric acid ratio is needed to fully dissolve the acid in the supercritical phase and to form CO_2-philic $UO_2(NO_3)_2(TBP)_2$ complexes. The resulting hydrogen-bonding and solvation patterns are analyzed. The results are consistent with experimental observations and provide microscopic views of this important extraction system.

Introduction

Supercritical CO_2 "SC−CO_2" can be used as a promising ecological alternative in liquid−liquid extraction systems.[1,2] This is of particular interest in the context of nuclear waste partitioning, which is generally initiated from aqueous solutions of metal ions, obtained by the dissolution of irradiated material in concentrated nitric acid solutions. Examples of metal extraction to SC−CO_2 from solid or liquid matrices involve extraction of metallic, lanthanide, and actinide cations by β-diketonate ligands, of strontium by crown ethers, or of UO_2^{2+}, Th^{4+}, lanthanides, or heavy metals by organophosphorus ligands.[3] Recently, a new technique for dissolving solid uranyl dioxide in SC−CO_2 with the CO_2-philic TBP·HNO_3 complexant without requiring dissolution by acid in water has been reported.[4−9] This extraction technology appears promising for effective processing with marked reduction in waste generation because no aqueous solutions and organic solvents are involved and phase separation can be achieved easily by depressurization. It is based on the "homogeneous" introduction of nitric acid with TBP in SC−CO_2, leading to UO_2 dissolution and conversion to UO_2^{2+}. As in classical extraction, uranyl is complexed with TBP, forming $UO_2(NO_3)_2(TBP)_2$ neutral complexes that are highly soluble in SC−CO_2.

Concentrated nitric acid contains a large amount of water (up to 30% for "pure" nitric acid) and has a low solubility in SC−CO_2. Solubilization in SC−CO_2 is achieved by shaking TBP with a concentrated nitric acid solution, likely leading to the formation of $TBP(HNO_3)_x(H_2O)_y$ adducts. The x and y proportions depend on the relative amounts of TBP and nitric acid. Typically, x can be up to 2.5 and y varies between 0.4 and 0.8, on the average.[8] Two types of complexes, with x = 0.7 and 1.8, respectively, have been characterized.[8] The complex with a HNO_3/TBP ratio of 0.7 was found to cause cloudiness of the supercritical fluid phase, indicating the formation of small water droplets released from the complex. The mechanisms of nitric acid solubilization by TBP and of the resulting uranium dissolution and complexation in the SC−CO_2 are not well known at the microscopic level.

Computer simulations[10] contribute to our understanding of solvation patterns and what happens in ion extraction. We recently reported the first molecular dynamics (MD) investigations on water/SC−CO_2 interfaces, either neat or in the presence of salts and extractant molecules such as calixarenes, crown ethers, and cryptands.[11] Inspired by the "green" (ecological) version of the PUREX (plutonium uranium extraction) process in which the organic phase is replaced by SC−CO_2, we also investigated the uranyl complexation and extraction by TBP from pH-neutral versus acidic solutions, focusing on the water/CO_2 interface.[12−14] In this paper, we report MD simulations of SC−CO_2 solutions containing various amounts of TBP, water, nitric acid, and uranyl nitrates with the aim of exploring to which extent TBP promotes the dissolution of nitric acid and whether the complexation of uranyl will take place in this medium, in relation to the recent work from Wai et al.[7,8] The simulations start from "random" positions of the solutes, including water (see Methods) which are thus "perfectly mixed" at the microscopic level (probably more than they are in reality). We want to investigate how they evolve spontaneously and relax and, in particular, how the acid, TBP, and uranyl nitrate species will distribute and interact once the equilibrium is reached. In all cases, we represent the acid by its neutral HNO_3 form, which should be dominant in the SC−CO_2 phase and a priori more soluble in this medium than the dissociated ionic form.

The simulated systems, noted **A** to **P**, are described in Table 1. Series **A**−**D** deals with nitric acid in the supercritical phase without TBP and can be used as a reference to investigate the

* Corresponding author. E-mail: wipff@chimie.u-strasbg.fr.

10.1021/jp051029y CCC: $30.25
Published on Web 05/20/2005

TABLE 1: Characteristics of the Systems Simulated in $SC-CO_2$

	systems	$n_{CO_2+H_2O}$[a]	box size (Å^3)	time[b] (ns)
A	120 HNO_3	901 + 123	43.6 × 41.8 × 52.6	2.0
B	120 HNO_3	902 + 20	43.5 × 41.6 × 53.9	2.0
C	120 HNO_3	901 + 0	43.9 × 41.8 × 50.1	2.0
D	120 HNO_3 + 6 $UO_2(NO_3)_2$	900 + 120	43.4 × 41.5 × 54.9	2.2
E	120 HNO_3 +30 TBP + 6 $UO_2(NO_3)_2$	901 + 125	43.4 × 41.6 × 61.8	7.3
F	120 HNO_3 +30 TBP	901 + 123	43.7 × 41.8 × 61.5	2.0
G	120 HNO_3 +60 TBP + 6 $UO_2(NO_3)_2$	900 + 120	43.9 × 41.8 × 70.1	3.0
H	120 HNO_3 +60 TBP	902 + 122	43.9 × 41.8 × 69.1	2.0
I	30 HNO_3 +60 TBP + 6 $UO_2(NO_3)_2$	899 + 120	43.9 × 41.9 × 64.9	2.6
J	30 HNO_3 +60 TBP	900 + 122	43.7 × 41.8 × 64.5	2.0
K	120 HNO_3+30 TBP + 6 $UO_2(NO_3)_2$	899 + 20	54.4 × 39.5 × 53.4	2.0
L	120 HNO_3 +60 TBP + 6 $UO_2(NO_3)_2$	899 + 20	43.9 × 41.8 × 69.0	2.0
M	30 HNO_3 +60 TBP + 6 $UO_2(NO_3)_2$	899 + 20	43.8 × 41.8 × 64.6	2.0
N	120 HNO_3 +30 TBP + 6 $UO_2(NO_3)_2$	900 + 0	43.4 × 41.6 × 60.8	3.0
O	120 HNO_3 +60 TBP + 6 $UO_2(NO_3)_2$	902 + 0	43.9 × 41.8 × 67.0	2.2
P	30 HNO_3 +60 TBP + 6 $UO_2(NO_3)_2$	902 + 0	43.9 × 41.9 × 62.4	2.0

[a] Number of CO_2 and H_2O molecules in the simulation box. [b] Demixing time after 1 ns of mixing.

effect of TBP (in systems **E**−**P**). **A**−**D** contain 120 HNO_3 molecules per simulation box, which corresponds to a concentration of about 2.2 mol/L. Systems **E**−**P** contain 30 or 60 TBPs, 6 $UO_2(NO_3)_2$ complexes, and different combinations of TBP, acid, and water. These systems allow us to investigate the effect of the acid/TBP ratio (from 4 to 0.5) and of the water/acid ratio (from 1 to 0) on the solubilization of acid in the supercritical phase and the complexation of uranyl nitrate. Solution models with two concentrations of nitric acid (120 vs 30 HNO_3 molecules) and three concentrations of water (∼120, 20, and 0 H_2O molecules), with or without uranyl salts, were prepared and simulated.

Because water and nitric acid likely compete to "solvate" TBP molecules in the organic phase, it is important to depict the interactions between the different partners correctly, in particular, the TBP···HNO_3 interactions should be strong enough to overcome the HNO_3···HNO_3, HNO_3···HOH, and H_2O···HOH ones. The first ones are thought to lead the dissolution of nitric acid by TBP, whereas the others likely prevent this process. For this purpose, we investigated these dimers as well as TBP-$(H_2O)_x(HNO_3)_y$ hydrogen-bonded trimers by quantum mechanical (QM) methods in the gas phase, and these results served as a reference to calibrate the charges used to simulate these species in $SC-CO_2$ solution by MD. In the QM calculations, TBP was mimicked by trimethyl phosphate TMP for computer time-saving purposes. Because TBP and TMP have similar dipole moments (3.02 vs 3.07 D) and donor numbers (DN = 23.0 vs 23.7 kcal/mol),[15] they should display similar hydrogen-bonding interactions with NO_3H or H_2O molecules.

Methods

Molecular Dynamics. The MD simulations were performed with the modified AMBER 5.0 software [16] where the potential energy is described by a sum of bond, angle, and dihedral deformation energies and pair-wise additive 1-6-12 (electrostatic + van der Waals) interactions between nonbonded atoms.

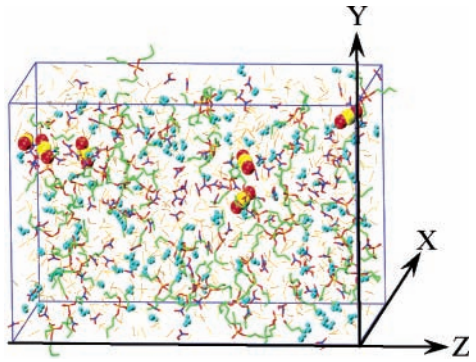

Figure 1. Simulation box.

$$U = \sum_{\text{bonds}} K_r(r - r_{\text{eq}})^2 + \sum_{\text{angles}} K_\theta(\theta - \theta_{\text{eq}})^2 + \sum_{\text{dihedrals}} V_n(1 + \cos n\phi) + \sum_{i<j}\left(\frac{q_{ij}}{R_{ij}} - 2\epsilon_{ij}\left(\frac{R^*_{ij}}{R_{ij}}\right)^6 + \epsilon_{ij}\left(\frac{R^*_{ij}}{R_{ij}}\right)^{12}\right)$$

The UO_2^{2+} and NO_3^- parameters are from Guilbaud and Wipff.[17] Water was represented with the TIP3P model.[18] For $SC-CO_2$, we used the parameters of Murthy et al.:[19] charges $q_C = 0.596$, $q_O = -0.298$ e; van der Waals parameters $R^*_O = 1.692$, $R^*_C = 1.563$ Å; and $\epsilon_O = 0.165$, $\epsilon_C = 0.058$ kcal/mol. All of the O−H, C−H, and C═O bonds of CO_2 were constrained with SHAKE using a time step of 2 fs. As in ref 13, the $UO_2(NO_3)_2$ salts were constrained to remain bound and neutral. The charges on HNO_3 and TBP were adapted in order to fit the quantum mechanics calculated TBP/HNO_3, TBP/H_2O, and HNO_3/H_2O interaction energies in the gas phase, retaining the TIP3P model for water. Another key feature concerns the preferred complexation of TBP over water by uranyl nitrate, and we made sure that the AMBER model also accounts for this trend.[20]

The MD simulations were performed in the NVT ensemble. The initial density of the CO_2 box was 0.80 g/cm^3, which is above the critical density (0.468 g/cm^3 at 304 K) and close to the density of 0.79 at 345 K and a pressure of 30 Mpa.[21,22] The temperature was monitored by separately coupling CO_2 and the solutes to a thermal bath at the reference temperature using the Berendsen algorithm[23] with a relaxation time of 0.5 ps. The systems were represented with 3D periodic boundary conditions, and the nonbonded interactions were calculated using a 15-Å cutoff with a reaction field correction for the electrostatic interactions.[24]

The solutes (including water molecules) were initially immersed in a box of CO_2 solvent. After 1000 steps of energy minimization, the system was mixed by MD for 1 ns at 700 K, scaling down the electrostatic interactions by a factor of 100 to enhance the mixing of hydrophobic and hydrophilic species. This lead to "chaotic mixtures" of CO_2 and solutes (see, for example, Figure 1). The "demixing" simulations were then initiated by resetting the temperature to 350 K and the dielectric constant of the medium to 1.0. Equilibration was attained in about 0.5 ns, but the dynamics was run for at least 2 ns (see Table 1). In one case (system **E**), the dynamics was pursued up to 7.3 ns. The results have been analyzed using our DRAW and MDS software,[25] and typical snapshots have been redrawn with VMD.£Humphrey, 1996 no. 7061. The hydrogen bonds between H and O atoms were selected based on structural

TABLE 2: Interaction Energies (in kcal/mol) in the Dimers and Trimers of TBP, H_2O, and HNO_3 Obtained with Different Levels of QM and FF Calculations. The Energy of the ABC Trimer Is Defined as $\Delta E = E_{ABC} - E_A - E_B - E_C$

		H_2O/H_2O	HNO_3/HNO_3	H_2O/HNO_3	TMP/(H_2O)	TMP/(HNO_3)	TMP/$(H_2O)_2$	TMP/H_2O/HNO_3	TMP/$(HNO_3)_2$
QM1	BLYP/6-31G* opt	−7.9	−10.0	−14.2	−10.4	−13.0	−19.9	−22.4	−23.1
QM2	BLYP/6-31G* opt + BSSE	−4.7	−6.4	−9.4	−7.0	−9.4	−9.7	−12.6	−15.4
QM3	BLYP/6-311 G++(d,p)[a]	−4.4	−6.3	−8.3	−6.7	−11.3	−11.7	−15.6	−18.2
QM4	BLYP/6-311 G++(d,p) opt	−5.5	−6.5	−8.0	−7.5	−11.9	−13.7	−16.7	−19.3
QM5	BLYP/6-311 G++(d,p) opt + BSSE	−4.7	−5.8	−6.7	−6.7	−10.7	−12.0	−14.8	−17.0
FF1	standard charges[b]	−6.6	−14.8	−13.4	−11.9	−21.9	−12.4	−11.0	−22.3
							−11.0	−21.1	−21.7
FF2	HNO_3-mod charges[c]	−6.6	−7.8	−8.6	−11.9	−15.3	−12.4	−9.2	−11.6
							−11.0	−12.0	−11.4
FF3	TBP-ESP 6-31G* charges[d]	−6.6	−7.8	−8.6	−7.5	−10.2	−7.4[e]	−10.5[e]	−9.3[e]
FF4	TBP-ESP 6-311G++(d,p) charges[d]	−6.6	−7.8	−8.6	−9.1	−11.7	−9.5	−8.2	−10.3
							−3.0[e]	−7.9[e]	−8.3[5]
FF5	ESP 6-31G* charges	−4.3	−8.0	−8.3	−6.4	−11.2	−5.8[e]	−5.7[e]	−10.4
									−9.7
FF6	ESP 6-311G++(d,p) charges	−5.1	−9.3	−9.6	−8.3	−14.1	−8.3	−7.7	−13.9
							−7.3	−13.6	−12.4

[a] BLYP/6-31G* optimization. [b] TBP ESP/MINDO − HNO_3 ESP HF/6-31G* − H_2O TIP3P. [c] TBP ESP/MINDO − HNO_3 mod − H_2O TIP3P. [d] TBP ESP − HNO_3 mod − H_2O TIP3P. [e] One H_2O or HNO_3 is not bonded to the Oxygen of TBP but to the O_{H_2O} or O_{NO_3H}.

criteria, that is, for H···O distances shorter than 2.4 Å. Calculations of the average density curves along the *Z* axis and analysis of hydrogen bonds were performed during the last 0.4 ns.

Quantum Mechanics. $TMP(HNO_3)_x(H_2O)_y$ complexes (x, y = 0, 1, or 2), the related hydrogen-bonded dimers were optimized with the Gaussian 98 software[26] at the density functional theory (DFT) level of theory (BLYP functional) using the 6-31G* and 6-311G++(d,p) basis sets. TMP (trimethyl phosphate), which models TBP was in the (gauche, gauche, trans) form. The interaction energies were calculated and corrected for basis-set superposition errors (BSSE).[27]

Results

We first describe the basic hydrogen-bonding interactions between TBP (modeled by TMP), H_2O, and HNO_3 in the gas phase, which constitutes a basis for empirical models used in the MD studies. This is followed by MD results on various mixtures of CO_2, water, TBP. and acid.

1. QM and Force-Field Studies on the Hydrogen-Bonded Dimers and Trimers Formed by TBP, H_2O, and HNO_3 in the Gas Phase. Table 2 reports the interaction energies of all of the hydrogen-bonded dimers between H_2O, HNO_3, and TMP as well as the trimers involving TMP as proton acceptor, from five computational protocols, noted QM1−QM5. Comparison of QM1 with QM2 and of QM4 with QM5 shows that BSSE effects can be quite substantial (up to ∼5 kcal/mol) and thus need to be taken into account. The effect of basis set for structure optimization (compare QM3 with QM4) is much smaller (∼0.5 kcal/mol). The five sets of QM calculations indicate that, in the series of dimers, TMP prefers HNO_3 over H_2O (by 3−4 kcal/mol) and the $H_2O\cdots H_2O$ dimer is somewhat less stable than the $HNO_3\cdots HNO_3$ dimer (by 1−2 kcal/mol). The sequence of binding energies of $H_2O\cdots HNO_3$ versus TMP···HOH is somewhat basis-set dependent. We thus consider the BSSE-corrected 6-311G++(d,p) results, which are a priori most satisfactory, and indicate increased H-bonding strengths in the series $(H_2O)_2 < (HNO_3)_2 < H_2O\cdots HNO_3 <$ TMP···HOH < TMP···HNO_3. We note that the binding energy calculated for TMP···HNO_3 (−10.7 kcal/mol) is identical to the value reported at the MP2/6-31G(d,p) level of theory.[28] The preference of TMP for nitric acid over water is also seen in the trimers, whose stability increases in the series $TMP(H_2O)_2 <$ TMP(H_2O)-$(HNO_3) <$ TMP$(HNO_3)_2$. Adding another HNO_3 molecule to the TMP(HNO_3) or TMP(H_2O) dimers is also more favorable (−7.6 and −9.2 kcal/mol, respectively) than the addition of one H_2O molecule (−5.1 and −6.2 kcal/mol, respectively). The stronger coordination of TMP to HNO_3, compared to H_2O can be seen in the optimized structures of the dimers and trimers (Figure 2) where the P═O···HO distances are ∼0.2 to 0.1 Å shorter with HNO_3 than with HOH. As expected, these are, for a given type of proton donor, somewhat longer (by ∼0.1 Å) in the trimers than in the dimers. The above results obtained with TMP should be valid for TBP, as confirmed by DFT-BLYP calculations (6-31G* basis with BSSE correction): both ligands display quasi identical interaction energies with H_2O (−7.0 vs −7.0 kcal/mol) as well as with HNO_3 (−9.4 vs −9.2 kcal/mol).

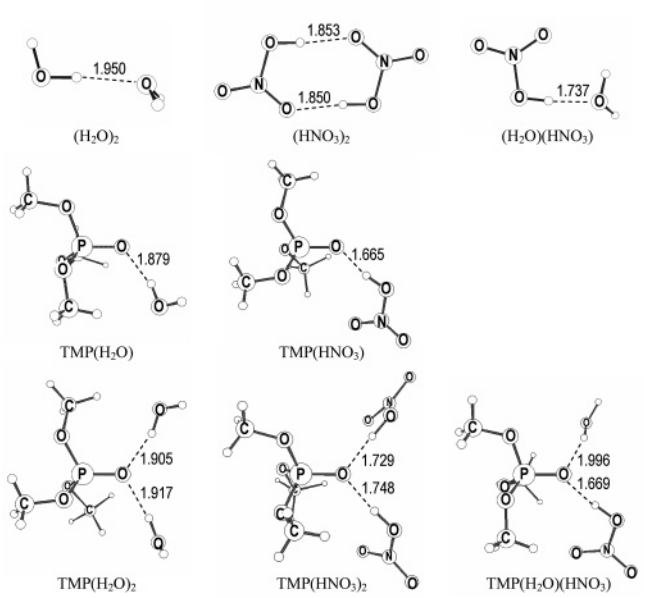

Figure 2. TMP, H_2O, and HNO_3 complexes. Optimized structures and $O_{TBP}\cdots H$ bonds distances (in Å) obtained from BLYP/6-311G++(d,p) calculations.

We attempted to reproduce these trends with the AMBER empirical force field (with TBP, instead of TMP) using various combinations of charge distributions, labeled FF1−FF6. These

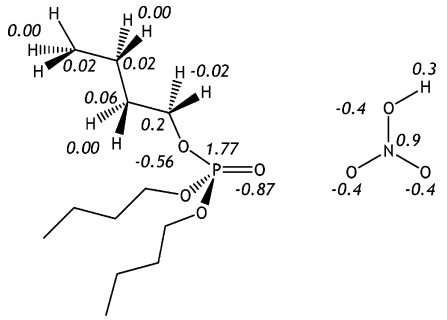

Figure 3. TBP and nitric acid charges used for the MD simulations (FF2 model).

are given in Figure S1. In FF1−FF4, the H_2O molecule is described by the TIP3P model ($q_O = -0.834$ e), whereas in FF5 and FF6, its charges are fitted from electrostatic ESP potentials (Merz −Kollman procedure implemented in Gaussian 98)[26] and are somewhat less polar ($q_O = -0.71$ e with the 6-31G* basis set and −0.76 e with the 6-311G++(d,p) basis set). For TBP and HNO_3, two QM models obtained from DFT-BLYP 6-31G* and 6-311G++(d,p) ESP (Merz−Kollman) calculations were considered. Standard (std) models from the literature (refs 12, 29, and 30 for TBP and 14 and 31 for HNO_3) were also tested. The std TBP model comes from MNDO calculations.[29] The resulting P═O bond is more polar than that with the two QM models and should thus form stronger H bonds. For nitric acid, the std model (from HF/6-31G* calculations with SPARTAN[32]) and a "modified" less polar version (vide infra) have also been considered. The dimers and trimers have been minimized by MD at low temperature (100 K) for 1 ns in the gas phase, starting from the BLYP optimized structures. The energy results are gathered in Table 2. Our main focus concerns the HNO_3 versus H_2O binding to TBP, and this is qualitatively well reproduced by models FF1−FF6 but clearly exaggerated by FF1 ($\Delta = 10$ kcal/mol, compared to the QM value of 4 kcal/mol). The results obtained with QM derived charges on all of the hydrogen-bonded partners (FF5 and FF6 models) are somewhat basis-set dependent and also exaggerate the preference for HNO_3 ($\Delta \approx 5$ to 6 kcal/mol). Furthermore, they underestimate the $H_2O\cdots H_2O$ energy and are thus less satisfactory to depict bulk water. This is why the FF5 and FF6 models were discarded for further MD studies. Among the remaining FF1−FF4 models, based on TIP3P water, FF3 and FF4 depict the dimers satisfactorily but not the trimers which were found to dissociate during the MD minimization, presumably because the P═O group is not polar enough. However, the FF1 model clearly exaggerates the interactions involving HNO_3, presumably because its O−H bond is too "acidic" and polar: its charges are $O^{-0.526}-H^{0.463}$. The latter and the remaining nitric acid charges were thus stepwise adapted, leading to the more satisfactory modified model FF2 with $O^{-0.4}-H^{0.3}$ charges. This is why we finally retained the FF2 model (the TBP and acid charges are shown in Figure 3), which accounts for the HNO_3 over H_2O preference in the dimer with TBP ($\Delta = 3.4$ kcal/mol). For the trimers, the FF2 difference of 3.9 kcal/mol between $TBP(HNO_3)_2$ and $TBP(H_2O)_2$ is also reasonably close to the QM5 calculated value of 5.0 kcal/mol. FF2 also qualitatively accounts for the QM calculated sequence of dimers reported above. The interactions with TBP are somewhat stronger with the FF2 than with the QM5 models, which is favorable for the studied process of nitric acid solubilization by TBP.

2. MD Simulations on Pure Nitric Acid/Water Solution in $SC-CO_2$ (No TBP). We first simulated model solutions of HNO_3/water in $SC-CO_2$ at different acid/water ratios without TBP (systems **A**−**D**). The systems evolved differently during the simulations, depending on the amount of water. Typical snapshots are given in Figure 4 and the statistics of hydrogen bonds is summarized in Table 3.

We first consider system **A** with a HNO_3/H_2O ratio of 1:1. The water concentration (∼22%) is not far from the experimental one (30% in pure nitric acid) and can be thus considered as more realistic than that in drier systems **B** and **C**. After 2.2 ns of dynamics of **A**, the water and acid molecules, which were randomly dispersed aggregate via H bonds, forming a single droplet in the supercritical phase in the absence of TBP. The shape of the droplet is very irregular and far from being spherical. The statistical analysis shows that all 120 HNO_3 molecules are involved in hydrogen-bonding interactions: 26 are hydrogen bonded with another acid molecule and 97 are hydrogen bonded with water (58 $H_{ac}\cdots O_w$ plus 40 $O_{ac}\cdots H_w$ hydrogen bonds). Similarly, among the 123 H_2O molecules, about one-half (61) interact with water, whereas the other half (59) interact with HNO_3. We note that the dominant population of hydrogen bonds via acid···water interactions (97) also mirrors the highest interaction energy among the dimers in the gas phase. In condensed phases, however, the situation is more complicated because of multiple proton donor and acceptor capability of water and the acid. See, for instance, the large occurrence of $O_{ac}\cdots H_w$ hydrogen bonds, despite the weak interaction energy.[33]

The effect of decreased water concentration can be seen in simulations **A**−**D**, showing that the acid molecules self aggregate and that the number of $HNO_3\cdots HNO_3$ interactions increases: from 26 for system **A** (123 H_2O per box) to 38 for **B** (20 H_2O) and to 44 for **C**, which is anhydrous. In the latter case, HNO_3 molecules collapse together, forming small aggregates in the CO_2 phase. A visual inspection of the trajectories indicates that the acid is somewhat more diluted in the dry than in the humid solutions, which indicates that water reduces its solubility in CO_2.

When uranyl nitrate complexes are added to the most humid solution (compare systems **A** and **D**), the distributions of nitric acid and water are hardly affected. The majority of the water and acid molecules are aggregated in a single elongated droplet and uranyl salts concentrate at the border of or inside this droplet. The first coordination sphere of the uranyl ions is completed in the equatorial plane by HNO_3 molecules or with a nitrate anion shared with another $UO_2(NO_3)_2$ species, thus forming uranyl···nitrate···uranyl chains in a local water microenvironment. Thus, in the absence of TBP, there are microphases of acid and water and the complexes form oligomers, instead of diluting in $SC-CO_2$.

3. MD Simulations on the Effect of Adding TBP to Nitric Acid/Water Mixtures in $SC-CO_2$. Systems E−J. In this section, we investigate the effect of TBP addition to $SC-CO_2$ solution containing water, uranyl salts, and nitric acid, simulated for at least 2 ns. Systems **E**−**J** contain ∼120 H_2O molecules and 120 HNO_3 acid molecules, which are thus in a 1:1 ratio, and 30 or 60 TBP molecules, that is, an excess of acid over TBP. Some systems also contain 6 $UO_2(NO_3)_2$ species (**E**, **G**, and **I**). Different situations were finally observed, depending on the HNO_3/TBP ratio. Typical snapshots are given in Figures 5 and S2, and the statistics of hydrogen bonds and uranyl complexes with TBP are summarized in Table 3.

In the **E** and **F** systems (acid/TBP = 120:30), which differ only by the presence (**E**) or not (**F**) of $UO_2(NO_3)_2$, the majority of water and nitric acid molecules aggregate to form a

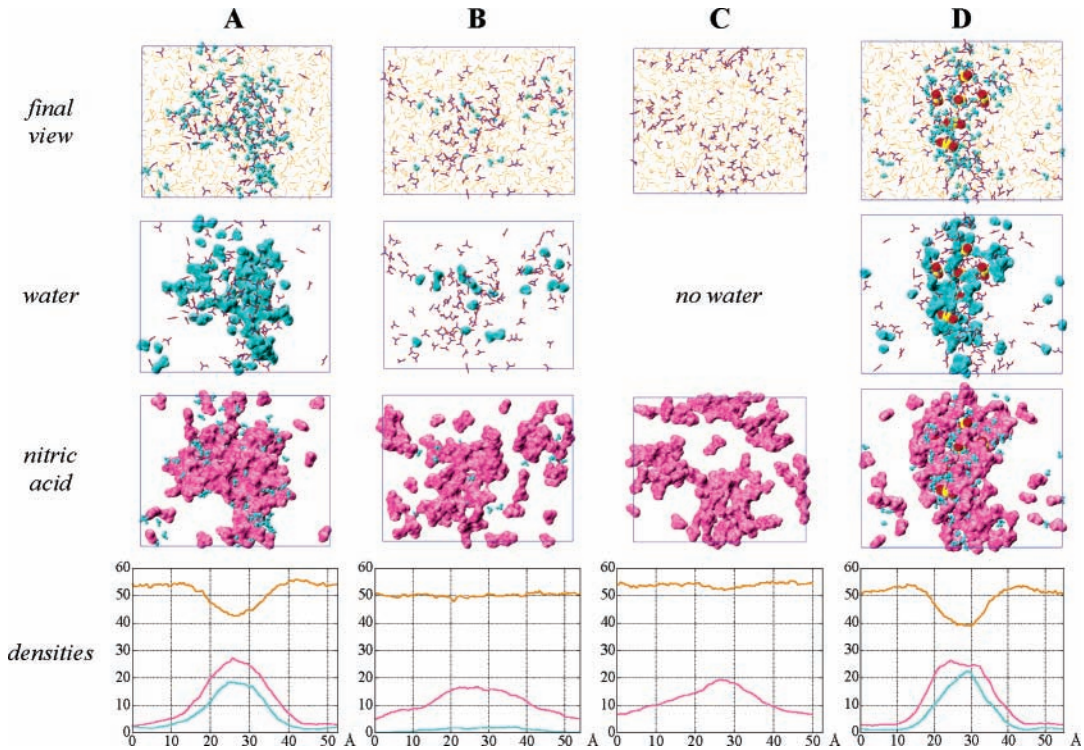

Figure 4. Final snapshots of systems **A**−**D** representing separately the surface of water and the surface of nitric acid. Density along the *Z* axis for CO_2 (*orange*), H_2O (*blue*), and HNO_3 (*pink*).

TABLE 3: Average Numbers of HNO_3···X and H_2O···X Hydrogen Bonds between the Different Species and Number of TBP Complexes with $UO_2(NO_3)_2$ Formed in SC−CO_2[a]

	H_{ac}/O_{ac}	H_{ac}/TBP		H_{ac}/H_w/TBP		H_{ac}/O_w	O_{ac}/H_w	H_w/TBP		O_w/H_w	$UO_2(NO_3)_2(TBP)_x$	
		1:1	2:1	1:1:1	1:2:1			1:1	2:1		$x=1$	$x=2$
A	26.0					57.8	39.7			61.0		
B	37.9					15.4	7.4			2.2		
C	44.0											
D	23.9					49.2	34.7			57.9		
E	17.3	4.7	10.6	5.5	0.7	48.7	25.7	2.5	7.2	62.3	4	2
E[b]	18.7	2.4	6.2	6.6	0.8	52.0	24.9	2.7	9.2	56.3	4	2
	(3.5)	(1.2)	(2.0)	(1.7)	(0.8)	(4.5)	(4.5)	(1.6)	(3.0)	(4.5)		
F	16.6	5.9	10.0	8.4	0.9	50.0	28.0	2.8	10.0	63.7		
G	9.8	11.8	10.8	13.0	1.2	46.6	18.6	8.4	16.8	45.3	1	5
H	10.5	11.7	15.2	14.1	1.8	48.5	17.8	8.1	27.6	54.5		
I	0.3	8.4	0.8	4.1	0.3	10.5	2.8	14.8	33.6	50.9	1	5
J	0.0	8.2	2.1	4.5	0.4	11.9	2.9	19.0	43.4	51.9		
K	24.1	7.1	17.4	3.9	0.0	14.9	5.3	1.3	1.0	1.2	1	3
L	15.1	23.3	33.2	5.2	0.4	11.3	3.5	3.1	3.6	2.5	3	3
M	0.0	21.8	0.0	0.2	0.0	0.5	0.3	14.1	7.4	0.0	1	5
N	28.2	5.5	27.6								2	4
O	15.5	25.7	43.2								0	6
P	0.0	23.5	0.0								0	6

[a] Unless otherwise specified, the averages are calculated between 1.6 and 2.0 ns. [b] Averages and fluctuations (in parentheses) calculated between 6.9 and 7.3 ns.

microdroplet of disk shape (∼25 Å in diameter and 7 Å in thickness) in the CO_2 phase. This droplet formed very quickly (in about 0.2 ns) and remained stable until the end of dynamics. The comparison with system **A** (no TBP) shows that TBP solubilizes part of the nitric acid molecules in the SC−CO_2 phase, via the formation of hydrogen-bonded dimers or trimers with H_2O or HNO_3 molecules. As a result, about half of the acid molecules sit in the organic phase and form mainly TBP-(HNO_3), TBP(HNO_3)$_2$, or TBP(HNO_3)(H_2O) adducts. The densities of the solutes of system **E** and **F** as a function of their *Z* position show clearly two main types of arrangements (Figures 5 and S2). One is composed mainly of a big domain of water and nitric acid (no CO_2) covered by TBP molecules, whereas other TBPs are "dissolved" in the CO_2 phase forming TBP···acid···water adducts. This suggests that the amount of TBP (30 TBPs) is not sufficient to further dissolve the water−acid aggregate.

Doubling the TBP concentration (compare systems **E** and **F** with 30 TBPs to **G** and **H** with 60 TBPs) markedly modifies the nature of the CO_2 phase and further solubilizes the acid (see snapshots and density curves in Figures 5 and S2). At the end of the dynamics, systems **G** and **H**, which contain a 120:60 proportion of HNO_3/TBP, are quite homogeneous. There is no more water−acid droplet, but a "uniform" dispersion of TBP, HNO_3, and H_2O molecules in the box. Following the Le Chatelier rule, as the number of TBP increases, one observes

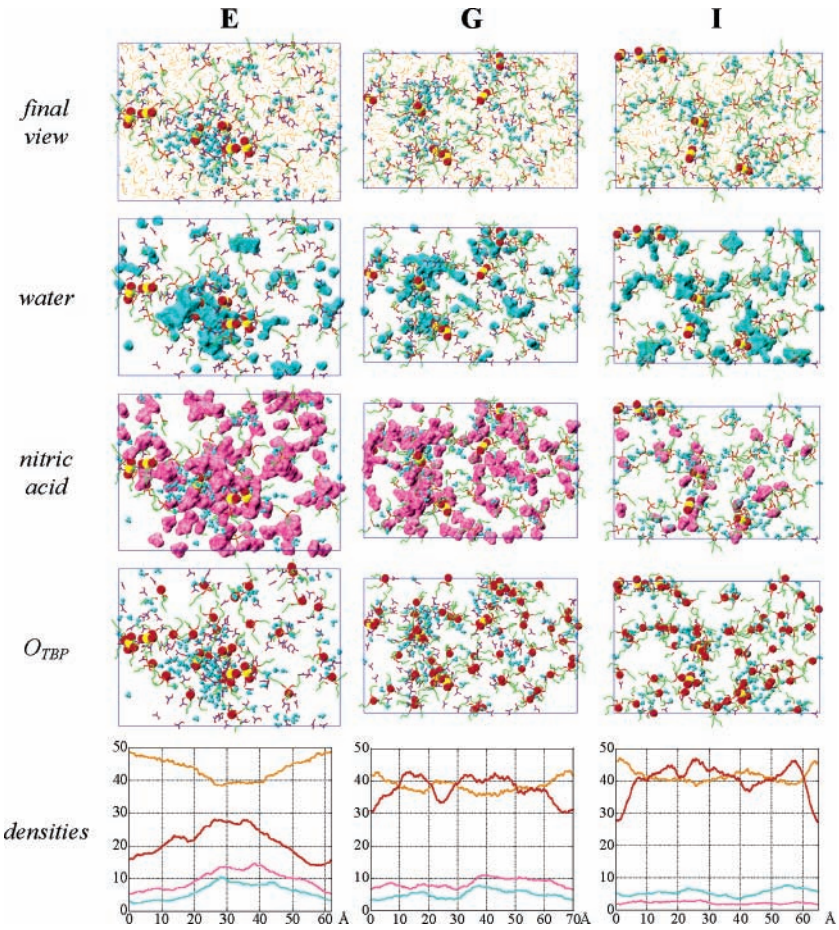

Figure 5. Final snapshots of the uranyl-containing **E**, **G**, and **I** systems, representing separately the surface of water, nitric acid, and the phosphoryl (TBP) oxygens. Linear density along the *Z* axis for CO_2 (*orange*), H_2O (*blue*), TBP (*red*), and HNO_3 (*pink*). A full version of the Figure, including the corresponding **F**, **H**, and **J** systems without uranyl is given in Figure S2.

an increasing number of TBP···HNO_3 adducts (from 21 with a 120:30 HNO_3/TBP ratio to 37 with a 120:60 ratio). TBP, which is well soluble in $SC-CO_2$, solubilizes nitric acid and water via the formation of hydrogen-bonded adducts. This phenomena is still more pronounced in systems **I** and **J** where TBP is in excess compared to the acid (the TBP/HNO_3 ratio is 60:30). In these systems, about half of the 30 HNO_3 molecules are H bonded to TBPs, whereas the other half are H bonded to water but nevertheless dissolved in the CO_2 phase. Looking at the computer graphics system reveals that much of these acid molecules sit in the second shell of TBP, forming TBP$(H_2O)_n$-(HNO_3) aggregates.

The statistical analysis of hydrogen bonds confirms the diversity of "complexes" (Table 3). TBP is involved in TBP$(HNO_3)_n$ and TBP$(HOH)_n$ dimers ($n = 1$) and trimers ($n = 2$), as well as in mixed TBP(HNO_3)(HOH) adducts, whose proportion varies with the concentrations of the different partners and will not be discussed in detail. The importance of water autoaggregation can be seen in the similar number of O_{wat}···H_{wat} interactions (about 50 to 60 in the systems **E** to **J**), which contrasts with the more variable numbers of acid···acid and water···acid interactions. Typical adducts are represented in Figure 6, showing dimers and trimers with TBP as well as more complex cooperative arrangements. See, for instance, the $(TBP)_2(H_2O)_2(HNO_3)_2$ "supermolecule", or the two forms of $(TBP)_2(H_2O)_2(HNO_3)$, that is, one where the acid coordinates to TBP and one where it coordinates in the second shell via one H_2O molecule. Such arrangements could hardly be detected by nearest-neighbor analysis.

Concerning the uranyl salts, they all spontaneously coordinated to TBP molecules during the dynamics to form $UO_2(NO_3)_2$(TBP) and $UO_2(NO_3)_2(TBP)_2$ complexes, as found at the water/CO_2 or water/chloroform interfaces or in water/CO_2 binary solutions.[12,30] In system **E** with 30 TBPs, the majority (4/6) of the complexes with TBP are of 1:1 type, and 2/6 are of 1:2 type, leaving uncomplexed TBP molecules hydrogen bonded with nitric acid and water. This suggests that this TBP concentration is too low to fully complex uranyls. Indeed, doubling the TBP concentration (from 30 TBPs in **E** to 60 TBPs in **G** and **I**) increases the proportion of $UO_2(NO_3)_2(TBP)_2$ complexes (from 2/6 to 5/6), at the detriment of $UO_2(NO_3)_2$(TBP) complexes (from 4/6 to 1/6), and this is favorable as far as their solubilization in $SC-CO_2$ is concerned. If one compares systems **G** and **I**, which differ by the acid concentration, one sees that the latter does not modify the extent of uranyl complexation.

4. On the Role of Water on the Nitric Acid Solubilization by TBP in $SC-CO_2$. Experimentally, concentrated liquid nitric acid contains a large amount of water, but the amount of water extracted to $SC-CO_2$ with TBP may be much smaller. This is why we decided to investigate the influence of the water concentration of TBP containing systems in which the water content was reduced (from ~120 to 0 H_2O molecules). Nitric acid is thus in excess over water, as observed in a TBP phase into which the concentrated acid has been dissolved.[8] Systems **K**−**M** contain "traces" of water (20 H_2O molecules), whereas systems **N**−**P** are dry, with no water at all. All systems **K**−**P** contain 6 $UO_2(NO_3)_2$ complexes.

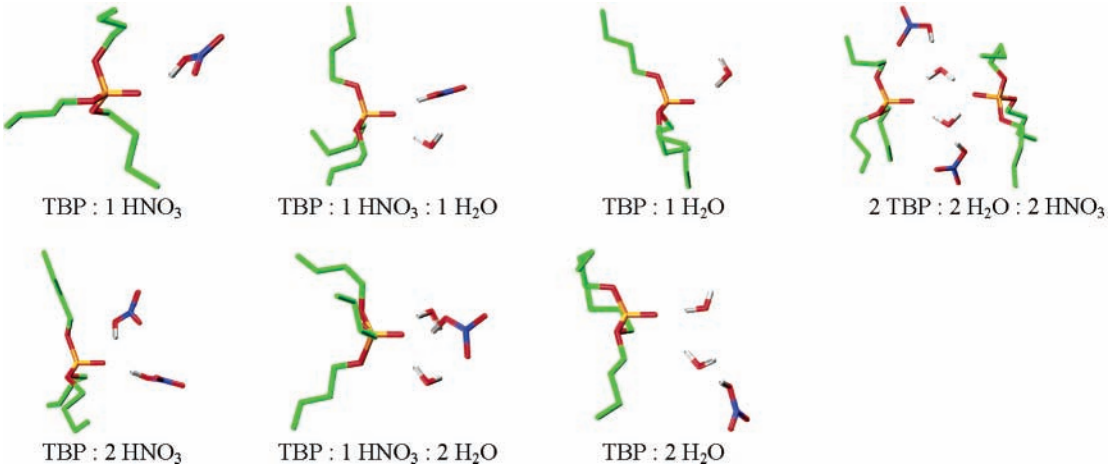

Figure 6. Snapshots of typical hydrogen-bonded adducts that formed spontaneously with TBP during the dynamics (system **J**).

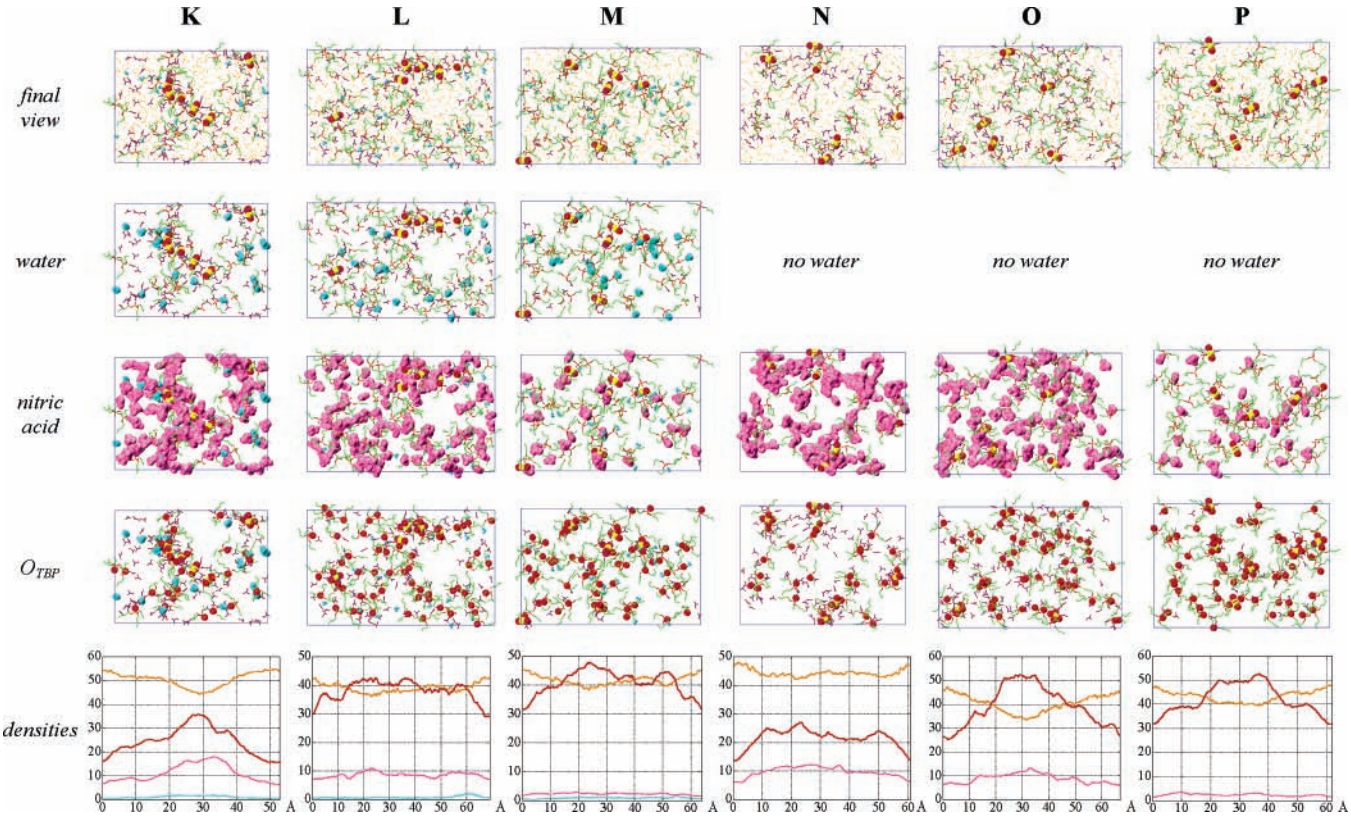

Figure 7. Final snapshots of systems **K**−**P** representing separately the surface of water, nitric acid, and the phosphoryl oxygens of TBP. Linear density along the *Z* axis for CO_2 (*orange*), H_2O (*blue*), TBP (*red*), and HNO_3 (*pink*).

Concerning the effect of TBP, systems **K**−**M** are found to display the same trends (see Figure 7 and Table 3) as their more humid analogues, **E**, **G**, and **I**. The distribution of nitric acid depends mainly on the amount of TBP. When it is too low, compared to the acid and water (system **K** with 30 TBPs), the latter components aggregate around the polar uranyl salts. When the number of TBPs increases from 30 to 60, the number of TBP···HNO_3 dimers also increases (from 7 in system **K** to 23 in **L**) and the acid and water molecules are more dispersed.

Concerning the effect of decreased humidity of the CO_2 phase, ones sees that the number of TBP···HNO_3 H bonds increases (the total, including monomers and homo + hetero dimers evolves from 33 in system **E** to 46 in **K** and 60 in **N**) because of the reduction of the competitive TBP···HOH interactions. The same trend is found in the systems with 30 HNO_3 and 60 TBP molecules (there are 14 H bonds in **I**, 22 in **M**, and 24 in **P**). This favors the acid dissolution. The number of H_2O···HNO_3 adducts also decreases, together with the possibility of aggregation and formation of acidic water droplets. This phenomenon is magnified in the dry systems, **N**−**P**, where all of the TBPs are either hydrogen bonded with HNO_3 molecules or complexed to form $UO_2(NO_3)_2(TBP)_2$ complexes exclusively.

Discussion

We report theoretical studies on the effect of TBP on nitric acid dissolution and uranyl complexation in supercritical CO_2, a complex phenomenon that depends on the concentration of the different partners. First, among the different combinations of hydrogen bonds involving nitric acid, water, and TBP (mimicked by TMP), QM calculations in the gas phase show that the TBP−acid interaction is strongest, in agreement with

another theoretical study.[34] This critical feature is accounted for by an empirical force-field representation of the potential energy used for MD studies. Several combinations of TBP, acid, water, and uranyl salts have been simulated by MD in $SC-CO_2$, allowing for pair-wise comparisons and revealing different microscopic behaviors. There is no firm criteria to define to what extent the acid will be dissolved in the supercritical phase, but visual inspection of the systems, as well as a statistical analysis of hydrogen-bonding interactions, demonstrate the effect of TBP. Indeed, without TBP, the HNO_3 molecules aggregate with water to form a microphase, and nitric acid therefore does not dissolve in CO_2. It can be surmised that ionic forms NO_3^- H_3O^+ of the acid, if present, would further "catalyze" the aggregation of water, thus preventing dissolution of the acid in $SC-CO_2$. This contrasts with the TBP-containing solutions where the percentage of nitric acid dissolved in the organic phase increases. Because the TBP···HNO_3 interactions are stronger than the HNO_3···HNO_3 and HNO_3···H_2O ones, TBP molecules are practically all H bonded to nitric acid or to water in the studied systems, forming a large variety of complexes during the dynamics. Many are of TBP$(HNO_3)_x$ or TBP$(H_2O)_x$ type (with $x = 1$ or 2) or mixed TBP$(HNO_3)(H_2O)_x$ with $x = 1$ or 2, but more complex supramolecular arrangements can be observed (Figure 6), which could hardly be detected by, for example, vibrational spectroscopy. As expected, one finds more TBP/HNO_3 than TBP/H_2O adducts at equal concentrations of acid and water. The total number and stoichiometry of hydrogen-bonded TBP adducts increases with the TBP concentration, following experimental observations.[7,8] The observed percentage of dimers is highest when the HNO_3/TBP ratio is smaller than one. When this ratio becomes larger than one, the number of trimers also increases.

It should be noted that hydrogen-bonded supermolecules are dynamic in nature, especially at the simulated temperature of 350 K. This can be seen, for example, in the case of system **E** by the important fluctuations (Table 3) as well the visual inspection at different times (see snapshots in Figure S3). Thus, pursuing the dynamics further from 2 to 7.3 ns leads to somewhat different numbers of hydrogen-bonded species, but the overall trends remain the same (see Table 3). In addition, the numbers of 1:1 and 1:2 uranyl complexes formed by TBP are identical after 2 ns and 7.3 ns of dynamics. We thus believe that the evolutions from one system to another are well captured after 2 ns of simulation.

According to the simulations, uranyl solutes, although polar, have little effect of the solubilization of nitric acid in the CO_2 phase, presumably because of their relatively low concentration. One remarkable result concerns their spontaneous complexation by TBP molecules during the dynamics, forming 1:1 and 1:2 complexes whose relative populations evolve with the TBP concentration. In the $UO_2(NO_3)_2(TBP)_2$ complexes, uranyl is shielded from solvent, and the latter are diluted in the $SC-CO_2$ phase. This contrasts with the unsaturated $UO_2(NO_3)_2$-(TBP) complexes that tend to oligomerize at low TBP concentration and are thus less CO_2-philic. Another point of interest concerns the role of water, which at high concentration catalyzes the acid condensation and prevents its dissolution in the CO_2 medium. In the extreme case of the dry solutions, a small amount of acid (systems **M** and **P** with 30 HNO_3 molecules) dilutes in the CO_2 phase via hydrogen-bonding interactions with an excess of TBP. When the acid is in excess over TBP, however, it aggregates without forming a well-defined droplet or microphase as in the humid conditions. What happens at other TBP, acid, and water concentrations or under different thermodynamic conditions (temperature, pressure) remains to be investigated. It is hoped that the microscopic views presented here will contribute to a better understanding of the complex process of uranyl complexation and nitric acid dissolution in $SC-CO_2$ by TBP.

Acknowledgment. We are grateful to IDRIS, CINES, Université Louis Pasteur, and PARIS for computer resources and to E. Engler for his kind assistance.

Supporting Information Available: Figures S1−S3. This material is available free of charge via the Internet at http://pubs.acs.org.

References and Notes

(1) Laintz, K. E.; Wai, C. M.; Yonker, C. R.; Smith, R. D. *Anal. Chem.* **1992**, *64*, 2875.
(2) Erkey, C. *J. Supercrit. Fluids* **2000**, *17*, 259−287.
(3) Wai, C. M.; Gopalan, A. S.; Jacobs, H. K. In *Supercritical Carbon Dioxide. Chapter1*; Gopalan, A. S.; Wai, C. M.; Jacobs, H. K., Eds.; Washington, 2003; pp 2−8.
(4) Samsonov, M. D.; Wai, C. M.; Lee, S. C.; Kulyako, Y.; Smart, N. G. *Chem. Commun.* **2001**, 1868−1869.
(5) Tomioka, O.; Meguro, Y.; Iso, S.; Yoshida, Z.; Enokida, Y.; Yamamoto, I. *J. Nucl. Sci. Technol.* **2001**, *38*, 461.
(6) Enokida, Y.; El-Fatah, S. A.; Wai, C. M. *Ind. Eng. Chem. Res.* **2002**, *41*, 2282−2286.
(7) Enokida, Y.; Yamamoto, I.; Wai, C. M. In *Supercritical Carbon Dioxide. Chapter 2*; Gopalan, A. S.; Wai, C. M.; Jacobs, H. K., Eds.; Washington, 2003; pp 10−22.
(8) Enokida, Y.; Tomioka, O.; Lee, S.-C.; Rustenholtz, A.; Wai, C. M. *Ind. Eng. Chem. Res.* **2003**, *42*, 5037−5041.
(9) Trofimov, T. I.; Samsonov, M. D.; Kulyako, Y. M.; Myasoedov, B. F. *C. R. Chim. Acad. Sci.* **2004**, *7*, 1209−1213.
(10) Allen, M. P.; Tildesley, D. J. *Computer Simulation of Liquids*.; van Gunsteren, W. F., Weiner, P. K., Eds.; Clarendon Press: Oxford, 1987.
(11) Schurhammer, R.; Berny, F.; Wipff, G. *Phys. Chem. Chem. Phys.* **2001**, *3*, 647−656.
(12) Baaden, M.; Schurhammer, R.; Wipff, G. *J. Phys. Chem. B* **2002**, *106*, 434−441.
(13) Schurhammer, R.; Wipff, G. In *Separations and Processes Using Supercritical Carbon Dioxide*; Gopalan, A. S., Wai, C., Jacobs, H., Eds.; ACS: Washington, DC, 2003; pp 223−244.
(14) Schurhammer, R.; Wipff, G. *New J. Chem.* **2002**, *26*, 229−233.
(15) Marcus, Y. *Ion Solvation*; Wiley: Chichester, U.K., 1985.
(16) Case, D. A.; Pearlman, D. A.; Caldwell, J. C.; Cheatham, T. E., III; Ross, W. S.; Simmerling, C. L.; Darden, T. A.; Merz, K. M.; Stanton, R. V.; Cheng, A. L.; Vincent, J. J.; Crowley, M.; Ferguson, D. M.; Radmer, R. J.; Seibel, G. L.; Singh, U. C.; Weiner, P. K.; Kollman, P. A. *AMBER 5*; University of California, San Francisco, CA, **1997**.
(17) Guilbaud, P.; Wipff, G. *J. Mol. Struct.: THEOCHEM* **1996**, *366*, 55−63.
(18) Jorgensen, W. L.; Chandrasekhar, J.; Madura, J. D.; Impey, R. W.; Klein, M. L. *J. Chem. Phys.* **1983**, *79*, 926−936.
(19) Murthy, C. S.; Singer, K.; McDonald, I. R. *Mol. Phys*. **1981**, *44*, 135−143.
(20) The force field models based on TIP3P water qualitatively account for the higher affinity of $UO_2(NO_3)_2$ for TBP, compared to H_2O, as modelled by the exchange reaction: $UO_2(NO_3)_2(H_2O)_2 + 2TBP \rightarrow UO_2(NO_3)_2(TBP)_2 + 2H_2O$. The calculated energies are −50.0 kcal/mol (with FF1 and FF2), −5.6 kcal/mol (FF3), and −21.9 kcal/mol (FF4). They follow experimental trends (Vdovenko, V. M. *Neorg. Khim.* **1957**, *2*, 1677). The force fields are defined in the text (Section 1 of Results).
(21) (a) Graham, B. F.; Lagalante, A. F.; Bruno, T. J.; Harrowfield, J. M.; Trengove, R. D. *Fluid Phase Equilib.* **1998**, *150*−*151*. (b) Graham, B. F.; Lagalante, A. F.; Bruno, T. J.; Harrowfield, J. M.; Trengove, R. D. *Fluid Phase Equilib.* **1998**, 829−838.
(22) Lagalante, A. F.; Hansen, B. N.; Bruno, T. J.; Sievers, R. E. *Inorg. Chem.* **1995**, *34*, 5781−5785.
(23) Berendsen, H. J. C.; Postma, J. P. M.; van Gunsteren, W. F.; DiNola, A. *J. Chem. Phys.* **1984**, *81*, 3684−3690.
(24) Tironi, I. G.; Sperb, R.; Smith, P. E.; van Gunsteren, W. F. *J. Chem. Phys.* **1995**, *102*, 5451−5459.
(25) Engler, E.; Wipff, G. In *Crystallography of Supramolecular Compounds*; Tsoucaris, G., Ed.; Kluwer: Dordrecht, The Netherlands, 1996; pp 471−476.
(26) Frisch, M. J.; Trucks, G. W.; Schlegel, H. B.; Scuseria, G. E.; Robb, M. A.; Cheeseman, J. R.; Zakrzewski, V. G.; Montgomery, J. A., Jr.; Stratmann, R. E.; Burant, J. C.; Dapprich, S.; Millam, J. M.; Daniels, A.

D.; Kudin, K. N.; Strain, M. C.; Farkas, O.; Tomasi, J.; Barone, V.; Cossi, M.; Cammi, R.; Mennucci, B.; Pomelli, C.; Adamo, C.; Clifford, S.; Ochterski, J.; Petersson, G. A.; Ayala, P. Y.; Cui, Q.; Morokuma, K.; Malick, D. K.; Rabuck, A. D.; Raghavachari, K.; Foresman, J. B.; Cioslowski, J.; Ortiz, J. V.; Stefanov, B. B.; Liu, G.; Liashenko, A.; Piskorz, P.; Komaromi, I.; Gomperts, R.; Martin, R. L.; Fox, D. J.; Keith, T.; Al-Laham, M. A.; Peng, C. Y.; Nanayakkara, A.; Gonzalez, C.; Challacombe, M.; Gill, P. M. W.; Johnson, B. G.; Chen, W.; Wong, M. W.; Andres, J. L.; Head-Gordon, M.; Replogle, E. S.; Pople, J. A. *Gaussian 98*, revision A.5; Gaussian, Inc.: Pittsburgh, PA, 1998.

(27) Boys, S. F.; Bernardi, F. *Mol. Phys.* **1970**, *19*, 553−566.

(28) Kim, Y.; Kim, H.; Park, J. *Bull. Korean Chem. Soc.* **2002**, *23*, 1811−1815.

(29) Beudaert, P.; Lamare, V.; Dozol, J.-F.; Troxler, L.; Wipff, G. *Solvent Extr. Ion Exch.* **1998**, *16*, 597−618.

(30) Baaden, M.; Burgard, M.; Wipff, G. *J. Phys. Chem. B* **2001**, *105*, 11131−11141.

(31) Berny, F.; Schurhammer, R.; Wipff, G. *Inorg. Chim. Acta* **2000**, *300*−*302*, 384−394.

(32) SPARTAN 5.0; Wave Function Inc.: Irvine, CA, **1997**.

(33) The interaction energy for the HON(O)O···HOH dimer is calculated to be only 1.5 kcal/mol (6-311G++(d,p) DFT-BLYP optimizations, with BSSE correction). See also Hart, J. R.; Thakkar, A. J. *J. Mol. Struct.: THEOCHEM* **2005**, *714*, 217−220.

(34) Kim, Y.; Park, C.-Y.; Kim, H. *Ind. Eng. Chem. Res.* **2005**, *44*, 3389−3395.